

Post common envelope binaries from SDSS. II: Identification of 9 close binaries with VLT/FORS2*

M.R. Schreiber¹, B.T. Gänsicke², J. Southworth², A.D. Schwope³, D. Koester⁴

¹ Departamento de Física y Astronomía, Facultad de Ciencias, Universidad de Valparaíso, Valparaíso, Chile

² Department of Physics, University of Warwick, Coventry CV4 9BU, UK

³ Astrophysikalisches Institut Potsdam, An der Sternwarte 16, D-14482 Potsdam, Germany

⁴ Institut für Theoretische Physik und Astrophysik, University of Kiel, 24098 Kiel, Germany
e-mail: Matthias.Schreiber@uv.cl

Received / Accepted

Abstract

Context. Post common envelope binaries (PCEBs) consisting of a white dwarf and a main sequence star are ideal systems to calibrate current theories of angular momentum loss in close compact binary stars. The potential held by PCEBs for further development of close binary evolution could so far not be exploited due to the small number of known systems and inhomogeneity of the sample. The Sloan Digital Sky Survey is changing this scene dramatically, as it is very efficient in identifying white dwarf/main sequence (WDMS) binaries, including both wide systems whose stellar components evolve like single stars and - more interesting in the context of close binary evolution - PCEBs.

Aims. We pursue a large-scale follow-up survey to identify and characterise the PCEBs among the WDMS binaries that have been found with SDSS. We use a two-step strategy with the identification of PCEBs among WDMS binaries in the first phase and orbital period determinations in the second phase. Here we present first results of our ESO-VLT/FORS2 pilot-study that has the target of identifying the PCEBs among the fainter ($g \gtrsim 18.5$) SDSS WDMS binaries.

Methods. From published SDSS catalogues we selected 26 WDMS binaries to be observed with ESO-VLT/FORS2 in service mode. The design of the ESO-VLT/FORS2 observations was to get two spectra per object separated by at least one night. We used the Na I $\lambda\lambda$ 8183.27, 8194.81 doublet to measure radial velocity variations of our targets and performed additional follow-up spectroscopy using Magellan-Clay/LDSS3 of two systems showing significant radial velocity variations. Using a spectral decomposition/fitting technique we determined the white dwarf effective temperatures and surface gravities, masses, and secondary star spectral types for all WDMS binaries in our sample.

Results. Among the 26 observed WDMS binaries we find 9 strong PCEB candidates showing clear ($\geq 3\sigma$) radial velocity variations, and we estimate the fraction of PCEBs among SDSS WDMS binaries to be $\sim 35 \pm 12\%$. We find indications for a dependence of the relative number of PCEBs among SDSS WDMS binaries on the spectral type of the secondary star. These results are subject to small number statistics and need to be confirmed by additional observations. The orbital periods of two PCEB candidates, SDSS J1047+0523 and SDSS J1414-0132, we measured to be 9.17 hrs and 17.48 hrs respectively.

Conclusions. This pilot study demonstrates that our survey is highly efficient in identifying PCEBs among the SDSS WDMS binaries, and will indeed provide the observational parameters that are necessary to constrain the theoretical models of close binary evolution.

Key words. accretion, accretion discs – instabilities – stars: novae, cataclysmic variables – stars: binaries: close

1. Introduction

The majority of all stars are born in binary or multiple star systems and a significant fraction of these will interact at some point during their lives. Once the more massive stars leaves the main sequence and depending on the initial conditions, dynamically unstable mass transfer or a tidal instability may force the system to enter the common envelope (CE) phase (see Taam & Ricker, 2006, for more details). In this phase a gaseous envelope around the entire binary forms and friction within the envelope is significantly reducing the binary separation. Since Paczyński (1976) it

is generally believed that virtually all close compact binary systems ranging from X-ray binaries to double white dwarf binaries or cataclysmic variables, to name a few, have formed through CE evolution. Willems & Kolb (2004) performed comprehensive binary population synthesis studies for white dwarf/main sequence binaries (WDMS), and find that dynamically stable mass transfer may produce some additional short orbital period ($P_{\text{orb}} \gtrsim 10$ days) systems primarily consisting of low-mass He white dwarfs ($0.1 \leq M_{\text{wd}} \leq 0.4 M_{\odot}$) and relatively massive secondary stars (up to $6 M_{\odot}$). In the vast majority ($\sim 75 - 99\%$) of cases, however, a CE phase is needed to produce short orbital period ($P_{\text{orb}} \lesssim 400$ days) WDMS.

From theoretical simulations we learned that the CE phase is probably very short, i.e. $\lesssim 10^3$ yrs, that the spiral in starts rapidly after the onset of the CE phase, and

Send offprint requests to: M.R. Schreiber

* Based on observations collected at the European Southern Observatory, Paranal, Chile under programme ID 078.D-0719. This paper includes data gathered with the 6.5 meter Magellan Telescopes located at Las Campanas Observatory, Chile.

that the expected form of post-CE planetary nebulae are bipolar (see e.g. Morris, 1981; Taam & Bodenheimer, 1989; Taam & Sandquist, 2000; Webbink, 2007, and references therein). Hydrodynamical studies have been carried for a number of parameters (e.g. Taam & Ricker, 2006, for a recent review), however, these expensive simulations cannot be used in population synthesis models. Instead simple equations relating the total energy of the binary before and after the CE phase are applied (e.g. Willems & Kolb, 2004). Usually, the CE phase is simply approximated by a parameterised energy (Webbink, 1984; Willems & Kolb, 2004) or angular momentum equation (Nelemans et al., 2000). Both descriptions differ significantly in the predicted outcome of the CE phase, i.e. the energy equation predicts a much stronger shrinkage than the angular momentum equation (Nelemans & Tout, 2005). In addition, in both prescriptions the efficiency to “use” the orbital energy (or angular momentum) to expel the envelope is uncertain. Hence, the CE phase is probably the least understood part of close binary evolution and currently intensively debated (for recent discussions of the CE phase see Nelemans & Tout (2005); Webbink (2007); Beer et al. (2007)).

Once the envelope is expelled, the evolution of the PCEB is mainly driven by angular momentum loss (AML) due to magnetic braking. Unfortunately, the two currently favoured prescriptions for magnetic braking (Verbunt & Zwaan, 1981; Andronov et al., 2003), differ by up to two orders of magnitude in the predicted angular momentum loss rate. Even worse, it is not clear whether magnetic braking is present in all PCEBs, or whether it terminates in systems where the secondary star is fully convective. In order to explain the orbital period gap observed in the period distribution of CVs, one in fact needs to assume the latter, known as “disrupted magnetic braking”, (e.g. King, 1988; Howell et al., 2001). In contrast to this, observations of single low mass stars do not show any evidence for such a discontinuity (e.g. Pinsonneault et al., 2002).

Significant progress in our understanding of the CE phase and AML in PCEBs certainly requires both continuous theoretical efforts and innovative observational input. The potential that a large sample of white dwarf plus main sequence PCEBs could provide in this context has been first realised by Schreiber & Gänsicke (2003). They showed that it is possible to determine the orbital period the PCEB had when it left the CE phase and the white dwarf temperature as well as the orbital period it will have when entering the next phase of interaction (becoming a cataclysmic variable). More recently, Politano & Weiler (2006) showed that the disrupted magnetic braking hypothesis can be tested by knowing the relative number of PCEBs among white dwarf/main sequence (WDMS) binaries as a function of secondary spectral type. Finally Schreiber et al. (2007) recently summarised that a representative sample of PCEBs could probably constrain the CE efficiency, the description of the CE phase, and the strength of magnetic braking.

Unfortunately, only a very limited number of PCEBs with known effective temperature and orbital period is currently available. The PCEB sample that Schreiber & Gänsicke (2003) analysed consisted of only 30 well-studied short-period WDMS known in 2002. Since then, e.g. Gänsicke et al. (2004), Morales-Rueda et al. (2005), van den Besselaar et al. (2007), Shimansky et al. (2006), Aungwerojwit et al. (2007), and Tappert et al. (2007) added additional systems and the current number

of well studied PCEBs is close to 50. The number of systems required to constrain close binary evolution is certainly much higher. Schreiber et al. (2007) estimate that about 200 PCEBs with known white dwarf temperatures, secondary star parameters, and orbital periods are needed.

The Sloan Digital Sky Survey (SDSS) is currently opening a new era of observational population studies for a wide variety of astronomical objects, including WDMS binaries. As by-product of the quasar search within SDSS, more than 1000 WDMS binaries have been identified already within Data Release 5 (Eisenstein et al., 2006; Silvestri et al., 2007; Southworth et al., 2007). Though very large, this set of WDMS binaries is still subject to selection effects, as it favours systems with bluish colours, i.e. hot white dwarfs. To compensate for this, we have initiated a dedicated WDMS identification programme as part of SDSS II-SEGUE, which targets systems with a strong contribution of the companion star (see Schreiber et al., 2007). In parallel, we have started the identification of PCEBs among the WDMS binaries identified by SDSS by means of a radial velocity survey. Rebassa-Mansergas et al. (2007, henceforth Paper I) presented a first set of 18 PCEB candidates from radial velocity variations detected among multiple SDSS spectra. In this paper we present VLT/FORS2 observations of 26 faint ($g \gtrsim 18.5$) WDMS binaries which led to the identification of 9 new PCEBs through radial velocity variations. The orbital periods of two of these PCEBs were determined from additional Magellan-Clay/LDSS3 observations. The structure of the paper is as follows. In Section 2 we describe the selection of the 26 VLT targets and the determination of their stellar parameters. Details on the observations and data reduction of the VLT and Magellan-Clay runs are given in Sect. 3. After describing our method of measuring radial velocities and determining orbital periods (Sect. 4) we discuss our results in the context of our large-scale PCEB survey.

2. Target Selection and Stellar parameters

For this project, we selected 26 WDMS binaries with $i < 19.5$ and visible from Paranal from the SDSS Data release 5 (DR5, Adelman-McCarthy et al. 2007), using the lists compiled by Eisenstein et al. (2006); Silvestri et al. (2007); Southworth et al. (2007). Given the recently suggested test of disrupted magnetic braking (Politano & Weiler, 2006), we focussed this selection on WDMS binaries with intermediate M-type (M2–M5) companions. Table 1 lists the SDSS object names and the i magnitudes of our targets.

We have determined the stellar parameters of these 26 WDMS binaries following the method described in Paper I, with the only difference of now using spectra retrieved from Data Release 6, which have undergone a complete re-reduction that substantially improves the flux calibration (Adelman-McCarthy & for the SDSS Collaboration, 2007). For the sake of brevity, we provide here only a brief summary of the adopted procedures, for full details the reader is referred to Paper I. We first carry out a two-component fit to the SDSS WDMS spectra using libraries of observed white dwarf and M-dwarf template spectra, normalised to stellar surface fluxes. These template libraries are also compiled from SDSS DR6. This stage provides us with a spectral type for the companion star and a flux scaling factor for the M-dwarf template which, together with a spectral type-radius relation, yields

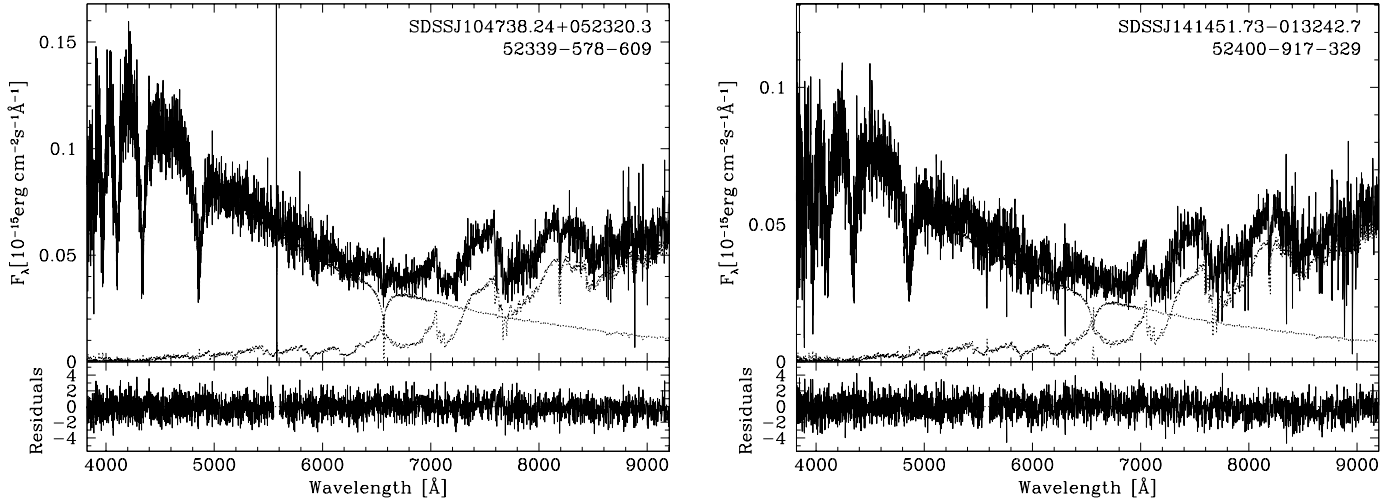


Figure 1. Two-component fits to the 2 PCEBs SDSS J1047+0523 and SDSS J1414-0132, for which we determined orbital periods from Clay/LDSS3 spectroscopy. Top panels: the WDM spectra (black lines) along with the white dwarf and M-dwarf templates (dotted lines). The MJD-PLT-FIB identifiers of the two SDSS spectra are also given. Bottom panels: residuals from the fit.

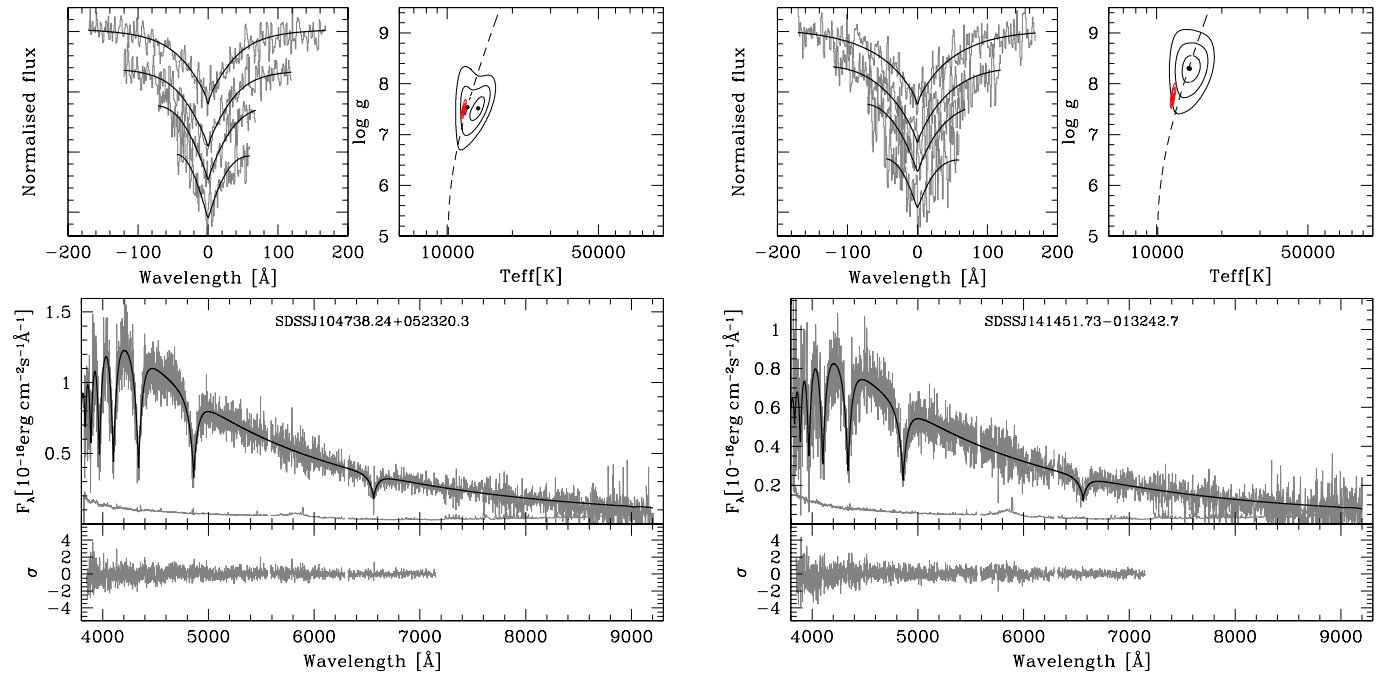


Figure 2. Spectral model fits to the white dwarf components of SDSS J1047+0523 and SDSS J1414-0132, obtained by subtracting the best-fit M-dwarf template from their SDSS spectra. Top left panels: normalised H β to H ϵ line profiles (top to bottom, gray lines) along with the best-fit white dwarf model (black lines). Top right panels: 1, 2, and 3 σ χ^2 contour plots in the $T_{\text{eff}} - \log g$ plane. The black contours refer to the best line profile fit, the red contours to the fit of the whole spectrum. The dashed line indicates the location of maximum H β equivalent width in the $T_{\text{eff}} - \log g$ plane, dividing it into “hot” and “cold” solutions. The best-fit parameters of the “hot” and “cold” normalised line profile solutions and of the fit to the 3850 – 7150 Å range are indicated by black and red dots, respectively. Bottom panels: the white dwarf spectrum and associated flux errors (gray lines) along with the best-fit white dwarf model (black lines) to the 3850 – 7150 Å wavelength range (top) and the residuals of the fit (gray line, bottom).

a distance estimate. In a second step, we subtract the best-fit M-dwarf template from the WDM spectra, and fit the residual white dwarf spectra with a standard χ^2 method for variable white dwarf effective temperature (T_{eff}) and surface gravity ($\log g$), using a grid of pure-hydrogen (DA) model spectra computed with the code of Koester et al.

(2005)¹. Two flavours of white dwarf fits were carried out for each object: (1) a fit to the normalised line profiles.

¹ We limit the spectral fitting to DA white dwarfs, but provide a spectral type of the companion for the two helium atmosphere (DB) WDMs binary in our sample.

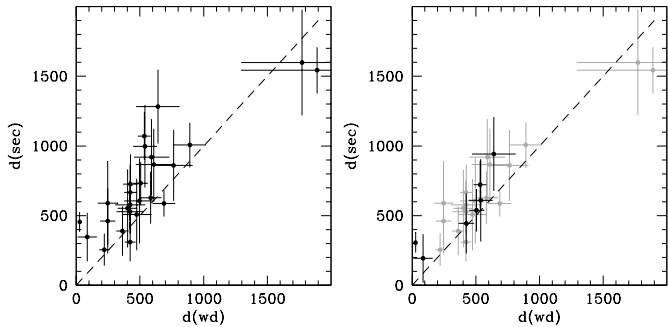


Figure 3. Distances of the 24 WDMS binaries in Table 1 that contain a DA white dwarf. The spectral modelling (Sect. 2) provides two independent distance estimates for the individual stellar components. Nine systems have $d_{\text{sec}} > d_{\text{wd}}$ by more than 1σ . Adopting secondary star spectral types later by one class brings most of them onto the $d_{\text{sec}} = d_{\text{wd}}$ relation. An earlier appearance of the spectral type determined from an optical spectrum may be related to stellar activity. See Paper I for additional discussion.

Due to the degeneracy in Balmer line equivalent width as a function of temperature two acceptable fits are usually found, a “hot” and a “cold” solution. (2) a fit to the continuum plus lines over the range $3850 - 7150 \text{ \AA}$. The parameters from this fit are subject to substantial systematic uncertainties due to inaccuracies in the *spectral slope*, and we only use them to break the degeneracy between the “hot” and “cold” line profile solutions. Examples of the spectral decomposition and of the white dwarf fits are shown in Fig. 1 and Fig. 2.

We then used an updated version of the tables in Bergeron et al. (1995)², which incorporate the structure and evolution calculations of Wood (1995) and Fontaine et al. (2001), to compute white dwarf masses and radii from T_{eff} and $\log g$. Finally, the white dwarf radii and flux scaling factors of the white dwarf models yield a second distance estimate. Statistical errors on the different properties are propagated through this process, but should be considered with some caution as additional systematic uncertainties are not easy to quantify. The resulting stellar parameters are listed in Table 1. Inspection of Fig. 3 (left panel) shows that in about one third of the systems the distance estimate based on the fit of the secondary star exceeds that based on the white dwarf fit by a significant ($> 1\sigma$) factor. A similar ratio of systems with $d_{\text{sec}} > d_{\text{wd}}$ has been found in the much larger sample analysed in Paper I, which also discusses in detail possible explanations for this finding. Our favoured hypothesis from Paper I is that stellar activity causes large scatter in the spectral type-radius relation of low-mass stars (in fact, larger than the scatter in their mass-radius relation that is subject to thorough investigations, e.g. Ribas 2006; López-Morales 2007), with a tendency for spectral types too early for their radius. In the right-hand panel of Fig. 3, we show that adopting secondary stars of one spectral class later than in Table 1 brings the nine systems which had $d_{\text{sec}} > d_{\text{wd}}$ on, or close to, the $d_{\text{sec}} = d_{\text{wd}}$ relation.

A final note concerns SDSS J2324–0931, which contains a DB white dwarf. The DR3 SDSS spectrum of

SDSS J2324–0931 was analysed by van den Besselaar et al. (2005) who adopted a method similar to our spectral decomposition, i.e. fitting the WDMS spectrum with the combination of observed white dwarf and M-dwarf templates. Different to our approach, they fixed the system distance to be the same for both stars. Their analysis resulted in $T_{\text{eff}} = 36815$, $\text{Sp}(2) = \text{M3V}$, and $d = 911 \text{ pc}$. Our spectral decomposition results in $\text{Sp}(2) = \text{M4V}$ and $d = 633 \pm 188 \text{ pc}$. Forcing the spectral type to M3V, we obtain a distance of $879 \pm 140 \text{ pc}$. Given that the typical uncertainty in the spectral type is one spectral class, the two results are hence consistent.

3. Observations

3.1. VLT/FORS2

Intermediate resolution spectroscopy of 26 WDMS binaries were obtained between August 16, 2007 and March 26, 2007 with FORS2 on the VLT/UT1 (Antu). The exposure time was 900sec for all objects. The observations were carried out using the 1028z grism and a $1''$ slit, resulting in a spectral coverage of $7830 - 9570 \text{ \AA}$. The images were processed using the STARLINK packages FIGARO and KAPPA, and the spectra were optimally extracted (Horne, 1986) using the PAMELA package (Marsh, 1989). From measurements of the FWHMs of sky lines we find our observations have a resolution of approximately 2.5 pixels (2.2 \AA) at 8200 \AA . Wavelength calibration of the extracted spectra was done using only sky emission lines. The wavelengths of good sky lines were obtained from the atlas of Osterbrock et al. (1996, 1997). 37 sky lines were included, and fitted with a fifth-order polynomial. The rms scatter around the fit was 0.11 \AA , so the statistical uncertainty in the wavelength scale is 0.04 \AA (Marsh et al., 1994). Finally, the spectra were flux-calibrated and compensated for telluric absorption using a spectrum of the standard star Feige 110.

The Phase II design of these observations was to obtain two spectra per object, separated by at least one night, in order to probe for radial velocity variations. Due to poor atmospheric conditions, additional repeat observations were obtained for several targets, while two objects only got one FORS2 spectrum each.

3.2. Magellan-Clay/LDSS3

Follow-up spectroscopy of two PCEBs identified from the FORS2 data, SDSS J1047+0523 and SDSS J1414–0123, were obtained over the period 2007 May 17–20 using the Magellan Clay telescope equipped with the LDSS3 imaging spectrograph. Seeing and transparency were highly variable. We adjusted the exposure times accordingly, ranging from 500–900sec for SDSS J1047+0523 and 750–1200sec for SDSS J1414–0123. We used the VPH_Red grism and OG 590 order-sorting filter. The detector was an unbinned STA $4k \times 4k$ pixel CCD read out by two amplifiers. A $0.75''$ offset slit gave a wavelength coverage of $5800 - 9980 \text{ \AA}$ at a reciprocal dispersion of 1.2 \AA px^{-1} . We took flat-field images at each sky position whilst observing as this was needed to remove the effects of fringing at redder wavelengths. The dispersed images were processed using the same software as for the VLT observations. Measurements of the FWHMs of the sky lines indicate that our observational setup gave a resolution of approximately 4 pixels

² <http://www.astro.umontreal.ca/~bergeron/CoolingModels/>

Table 1. Stellar parameter of the 26 WDMS binaries observed with FORS2, as determined from spectral modelling (Sect. 2). Upper limits on the orbital periods for the nine PCEBs identified by our VLT/FORS2 observations are calculated as described in Sect. 5.1

System (SDSS J)	MJD-plate-fibre	i	T [K]	$\log g$	$M_{\text{wd}}[M_{\odot}]$	$d_{\text{wd}}[\text{pc}]$	Sp	$d_{\text{sec}}[\text{pc}]$	notes
001726.63–002451.1	52559-1118-280	18.3	12828± 2543	8.00±0.46	0.61±0.29	423±119	4	577±171	
–	52518-0687-153	18.3	13588± 1803	8.11±0.39	0.68±0.25	423±107	4	529±157	
022835.92–074032.3	51908-0454-534	18.7	13588± 948	7.76±0.17	0.48±0.09	423± 43	6	311±140	
032038.72–063822.9	51924-0460-432	18.7	11045± 479	8.49±0.33	0.91±0.19	247± 61	5	461±232	1, $P_{\text{orb}} \leq 143.1$ d
081959.20+060424.2	52962-1296-138	19.2	15782± 1422	7.67±0.34	0.45±0.17	764±150	4	860±255	
083354.84+070240.1	52963-1297-511	18.5	16336± 730	8.03±0.16	0.63±0.10	424± 45	4	666±198	1, $P_{\text{orb}} \leq 14.7$ d
085542.49+044717.7	52670-1190-512	19.1	10073± 336	8.46±0.43	0.89±0.25	247± 77	5	589±297	1, $P_{\text{orb}} \leq 61.9$ d
092451.63–001736.4	52000-0474-175	17.6	24163± 1359	7.82±0.20	0.54±0.11	688± 89	3	588± 94	
093904.03+051114.8	52710-0993-296	19.2	12681± 1406	7.69±0.42	0.44±0.23	591±139	4	919±273	
095108.74+025507.5	51908-0481-419	18.5	13432± 1007	7.80±0.22	0.50±0.12	425± 57	4	726±215	
100953.69–002853.4	51909-0270-181	19.0	21535± 1927	8.35±0.32	0.84±0.19	609±141	4	867±257	
104358.59+060320.9	52643-1000-055	18.6	11565± 536	8.39±0.24	0.85±0.15	220± 39	6	256±115	
104738.24+052320.3	52339-0578-609	18.7	12392± 1847	7.54±0.42	0.38±0.20	474±111	5	508±256	1, 2, $P_{\text{orb}} < 0.8$ d
110151.34+122241.5	53119-1603-492	18.8	20331± 817	7.83±0.15	0.53±0.08	534± 50	3	1071±171	
112623.87+010856.8	51614-0281-402	17.5	16717± 781	7.91±0.18	0.57±0.10	505± 57	2	733±152	
122208.48+093406.2	52672-1230-73	18.3	30419± 2053	7.34±0.49	0.38±0.18	1891±599	0	1543±166	4
125250.03–020608.1	51694-0338-343	18.5	22037± 2333	8.29±0.38	0.80±0.23	641±171	2	1282±265	
141451.73–013242.7	52400-0917-329	19.0	14065± 1452	8.31±0.27	0.80±0.17	402± 77	5	552±278	1, 3, 6, $P_{\text{orb}} < 3.4$ d
142541.32+023047.4	51999-0535-348	18.9	13127± 1014	7.91±0.22	0.56±0.13	362± 48	6	390±176	
150657.58–012021.7	52426-0922-536	18.4	15782± 1005	7.72±0.24	0.47±0.13	584± 85	4	629±187	1, $P_{\text{orb}} < 9.1$ d
204541.90–050925.7	52145-0635-439	18.7	26801± 1432	7.78±0.22	0.53±0.11	892±127	3	1007±160	1, $P_{\text{orb}} < 49.1$ d
205059.37–000254.3	52466-0982-567	19.2	18330± 1169	8.27±0.24	0.78±0.15	539± 93	4	998±296	
212320.74+002455.5	52523-0987-484	19.2	12250± 1794	7.47±0.42	0.35±0.19	496±119	5	606±305	1, $P_{\text{orb}} < 0.4$ d
215614.57–000237.4	52078-0371-025	18.5	7910± 926	9.50±0.74	1.37±0.21	86± 76	5	346±174	1, 4, 6, $P_{\text{orb}} < 44.0$ d
220338.61–001750.7	52173-0372-034	18.7	32972± 1703	7.24±0.38	0.37±0.11	1772±477	1	1598±379	
231221.59+010127.0	51811-0381-570	17.3	–	–	–	–	3	455± 72	5
232438.31–093106.4	52203-0645-637	18.4	–	–	–	–	4	633±188	5

(1) PCEB candidate on the base of radial velocity variations detected among the available FORS2 and SDSS spectra; (2) $P_{\text{orb}} = 9.17$ h determined from Magellan-Clay/LDSS3 spectroscopy; (3) $P_{\text{orb}} = 17.48$ h determined from Magellan-Clay/LDSS3 spectroscopy; (4) blue component is faint, white dwarf parameter uncertain; (5) DB white dwarf; (6) poor quality spectrum.

(4.8 Å) at 8200 Å. Wavelength calibration was done using only sky lines, to increase observational efficiency. A total of 36 sky lines were fitted by a fifth-order polynomial. The rms scatter around the fit was 0.25 Å, so the statistical uncertainty is 0.09 Å. From this work and other studies we have found that reliable wavelength calibrations can be obtained from sky lines (see also Southworth et al. 2006), but that the scatter of the fit around the wavelength solution is quite a bit larger than for arc-lamp emission lines. In this case the statistical uncertainty is equivalent to 0.09 Å so the increased scatter is relatively unimportant.

Flux calibration and telluric line removal was performed using spectra of the standard star LTT 3218 obtained during the same observing run.

4. Radial velocity variations and orbital periods

We have used the strong Na I $\lambda\lambda$ 8183.27,8194.81 absorption doublet present in the spectra of all our targets to measure the radial velocities of the main-sequence companion stars. For this purpose, we fitted the wavelength of the Na I doublet using the sum of a linear slope for the continuum plus two Gaussians for the absorption lines. We fixed the separation of the two Gaussians to 11.54 Å corresponding to the laboratory value. Free parameters in the fit were the continuum flux level and slope, the wavelength of the doublet, the full-width at half maximum (FWHM) of the lines (both FWHM were fixed to vary together), and the amplitudes of the individual doublet components. The fits were carried

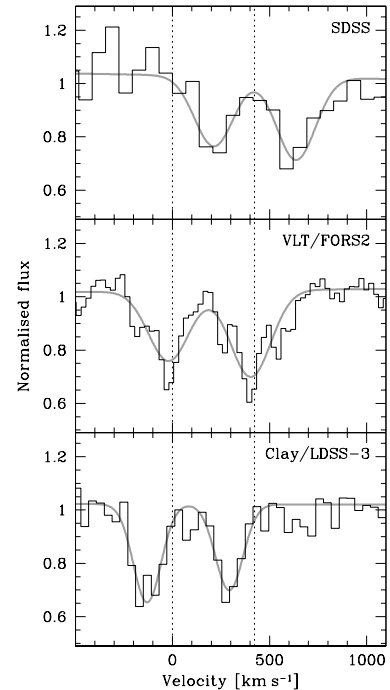


Figure 5. Examples of the double-Gaussian fits to the Na I $\lambda\lambda$ 8183.27,8194.81 line profiles in the SDSS, VLT/FORS2, and Clay/LDSS3 spectra of SDSS J1047+0523.

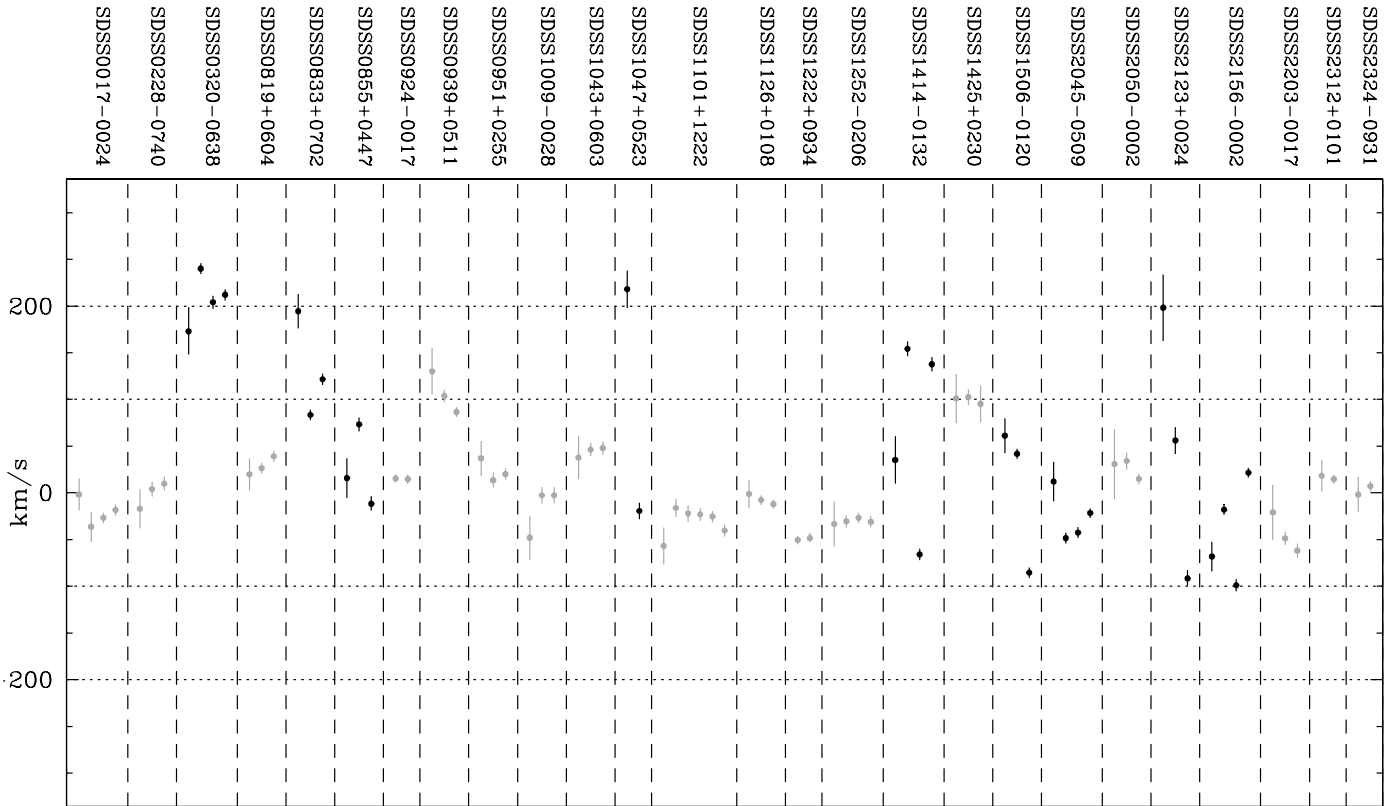


Figure 4. Radial velocities (Table 3 of our sample 26 WDMS binaries (Table 1), measured from the $\text{Na I } \lambda\lambda 8183.27, 8194.81$ doublets observed in their SDSS and FORS2 spectra. No SDSS radial velocities could be determined for SDSS J1252-0206, SDSS J1414-0132, and SDSS J2050-0002. See Fig. 5 for examples of the $\text{Na I } \lambda\lambda 8183.27, 8194.81$ fits. The systems with black symbols display radial velocity variations at a 3σ level.

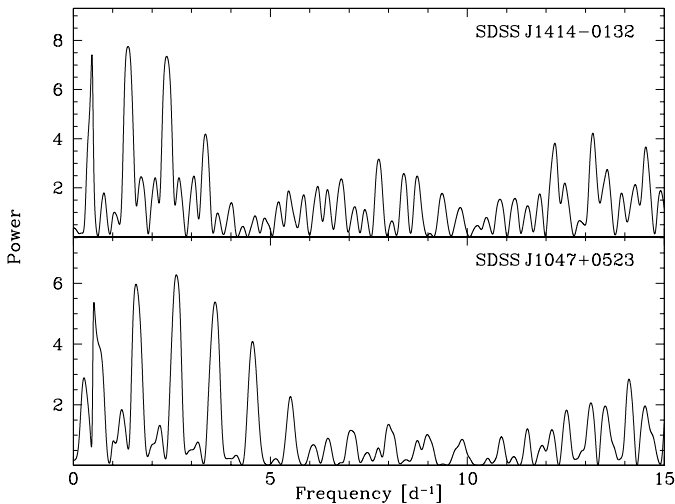


Figure 6. Scargle periodograms calculated from the $\text{Na I } \lambda\lambda 8183.27, 8194.81$ radial velocities measured in the LDSS3 spectra of SDSS J1414-0123 and SDSS J1047+0523.

out using the `fit/table` command in MIDAS. Examples of these fits are shown in Fig. 5. We added the uncertainty in the wavelength calibration in quadrature to the statistical errors in the wavelength of the Na I resulting from the double-Gaussian fit.

One system, SDSS J1222+0934, has an M0V secondary star, which exhibits no significant Na I absorption. For this

single object, we used the same method as above, but fitted three Gaussian lines of fixed separation and common width to the $\text{Ca II } \lambda\lambda 8498.02, 8542.09, 8662.14$ triplet.

We combined the radial velocities obtained from the FORS2 data with those measured from the DR6 SDSS spectra (Table 3). Comparing the individual radial velocities of each object, we define as a strong PCEB candidate all systems which show a radial velocity variation at a $\geq 3\sigma$ level. Applying this criterion, we identify 9 PCEB candidates among our target sample of 26 WDMS binaries (Fig. 4, Table 1).

The radial velocity variations of the companion stars in SDSS J1414-0132 and SDSS J1047+0523 were determined in an analogous fashion as described above from the Clay/LDSS3 spectroscopy. We then calculated Scargle (1982) periodograms from the mean-subtracted radial velocity measurements to establish the periods of the two WDMS binaries (Fig. 6). We carried out sine-fits to the radial velocities using the three highest aliases in the periodograms as initial value for the frequency, and report the resulting periods, γ -velocities and radial velocity amplitudes, as well as their errors and the reduced χ^2 values, in Table 2.

The lowest reduced χ^2 values as well as the lowest relative errors on the fit parameters are found for the periods corresponding to the highest peaks in the periodograms. We therefore conclude that the orbital periods of SDSS J1414-0132 and SDSS J1047+0523 are $P_{\text{orb}} = 17.48 \pm 0.07$ h and $P_{\text{orb}} = 9.17 \pm 0.02$ h. Folding the radial velocities

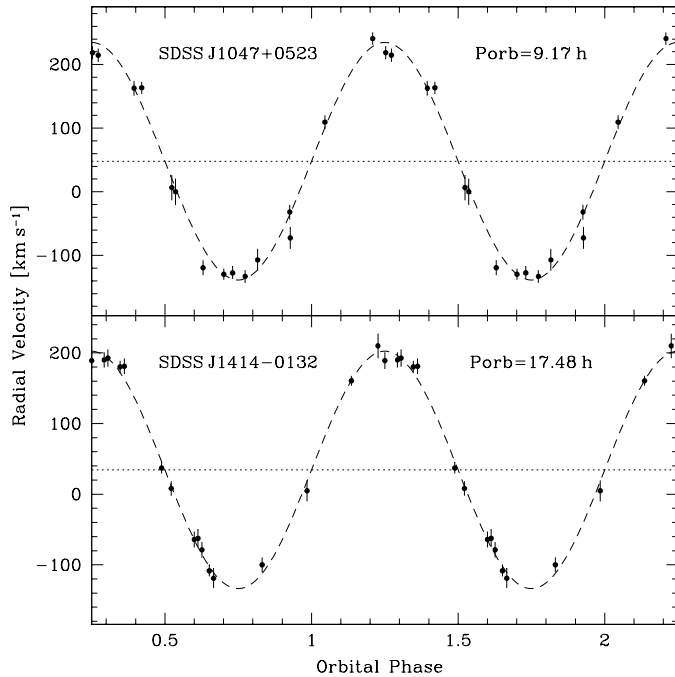


Figure 7. The $\text{Na I } \lambda\lambda 8183.27, 8194.81$ radial velocities of the companion stars in SDSS J1414-0132 and SDSS J1047+0523 folded over their respective orbital periods of $P_{\text{orb}} = 17.48$ h and $P_{\text{orb}} = 9.17$ h.

Table 2. Orbital periods, semi-amplitudes, and reduced χ^2 from sine-fits to the radial velocity data of SDSS J1047+0523 and SDSS J1414-0132 for the strongest three aliases in the periodograms shown in Fig. 6. The best-fit values are set in bold font.

System	P_{orb} [h]	K_2 [km s $^{-1}$]	γ [km s $^{-1}$]
SDSS J1047+0523	15.11 ± 0.12	195 ± 16	20 ± 11
	9.17 ± 0.02	187 ± 7	45 ± 5
	6.64 ± 0.04	181 ± 22	66 ± 17
SDSS J1414-0132	51.01 ± 0.53	371 ± 32	44 ± 12
	17.48 ± 0.07	168 ± 4	34 ± 3
	10.14 ± 0.09	152 ± 13	46 ± 10

over the neighbouring aliases results in substantially distorted non-sinusoidal periods. The LDSS3 radial velocities of SDSS J1414-0132 and SDSS J1047+0523 folded over their orbital periods are shown in Fig. 7.

Below we provide some comments on individual objects.

SDSS J0017-0024: Two SDSS spectra are available for this object, with radial velocities that are consistent at a 2σ level (Rebassa-Mansergas et al., 2007). We obtained two FORS2 spectra, which agree within their 1σ errors, confirming this system as a likely wide binary WDMS.

SDSS J1047+0523: Only a single VLT/FORS2 spectrum was obtained of this object. However, combining the radial velocity from the FORS2 spectrum with that measured

from the SDSS spectrum clearly identifies the system as a close binary.

5. Discussion

5.1. Orbital period limits

As in Rebassa-Mansergas et al. (2007) we determine an upper limit for the orbital period based on the measured radial velocity variations (Table 3). The orbital period as a function of the stellar masses, the binary inclination (i), and the radial velocity amplitude (K_{sec}) of the secondary follows from Kepler's 3rd law:

$$\frac{(M_{\text{wd}} \sin i)^3}{(M_{\text{wd}} + M_{\text{sec}})^2} = \frac{P_{\text{orb}} K_{\text{sec}}^3}{2\pi G} \quad (1)$$

Using the stellar parameters estimated in Sect. 2 from fitting the SDSS spectrum, assuming $i = 90^\circ$, and assuming the largest radial velocity difference measured for one particular system to be equal $2K_{\text{sec}}$, clearly gives an upper limit on P_{orb} . This method was used in Rebassa-Mansergas et al. (2007). Here we slightly improve this approach by using also the information provided by the times of observations. If the time delay between two spectra (Δt) is shorter than half the considered orbital period, the maximal radial velocity difference that could have been observed writes $2K_{\text{sec}} \sin(\pi \Delta t / 2P_{\text{orb}})$ and we modify Eq. (1) accordingly. Upper limits on the orbital period for the 9 PCEBs obtained with this method are given in Table 1.

5.2. The fraction of PCEBs among SDSS WDMS binaries

The first result of our PCEB survey will be the relative number of PCEBs among SDSS WDMS binaries. According to the derived limits on the orbital periods and the masses given in Table 1, the 9 close WDMS binaries identified in this paper clearly experienced a phase of mass transfer during the post main sequence evolution of the progenitor of the white dwarf. As mentioned in the Introduction, according to current WDMS binary population studies (with many uncertainties involved), the majority of all WDMS that formed through mass transfer interactions are expected to be PCEBs and only a small fraction of close systems may form through dynamically stable mass transfer. For the 9 PCEB candidates identified among our 26 WDMS systems dynamically stable mass transfer appears to be extremely unlikely as the white dwarf masses are rather high and the secondary spectral types are rather late (see Willems & Kolb, 2004, for more details). We therefore state to have identified 9 PCEBs.

In the first paper of this series (Rebassa-Mansergas et al., 2007) multiple SDSS spectroscopy has been used to identify 18 PCEB candidates among 101 WDMS binaries from the SDSS. Due to the low spectral resolution of SDSS spectra and the fact that in most of those 101 WDMS binaries only two SDSS spectra are available, the resulting PCEB fraction of $\sim 15\%$ certainly has to be considered as a lower limit on the true value. In this paper we identified 9 PCEBs among 26 SDSS WDMS binaries which gives a PCEB fraction of $35 \pm 12\%$, which is – as expected – substantially higher than our previous lower limit. The increased PCEB detection rate is probably the result of both, the higher resolution of

VLT/FORS2 and the fact that for most systems 3–4 spectra are available.

However, also in the case that more than 2 spectra are available exists a certain probability to sample similar orbital phases and also the observations presented here have a finite spectral resolution. In the context of our project on PCEB studies, it is important to understand possible selection effects in the established PCEB sample. We therefore developed a Monte-Carlo code to estimate the detection probability among SDSS WDMS binaries as a function of orbital period. For the purpose of this specific paper, we limit our analysis to the following assumptions: a mean radial velocity resolution of 6 km/s, stellar masses of $M_{\text{wd}} = 0.6 M_{\odot}$ and $M_{\text{sec}} = 0.3 M_{\odot}$, and uniformly distributed inclinations. For an assumed orbital period we randomly select the inclination, orbital phase, and times of observations. The only constraint on the latter being that the time differences should exceed 12 h and that all observations are performed in one semester. The randomly selected values are then used to calculate radial velocity differences. Repeating this exercise 10^4 times and counting the number of cases with a 3σ (alternatively 1 or 2σ) radial velocity variation gives the probability of detecting a PCEB with the assumed orbital period. Fig. 8 shows the results we obtain assuming that 2 or 3 spectra have been taken in one semester. In both cases the detection probability of different significance levels of radial velocity variations is shown. Of course, our strategy leads to a certain bias towards shorter orbital periods (and higher inclinations) because strong radial velocity variations are more likely to be detected in these systems. However, with three randomly taken VLT/FORS2 spectra our 3σ criterion is still ~ 15 – 30% sensitive to PCEBs with periods in the range of ~ 20 – 60 days. PCEBs with orbital periods longer than 70 days may hide among the systems with weak (2σ) radial velocity variations, and will require additional spectroscopy to be unambiguously identified. In general, Fig. 8 clearly shows that the fraction of PCEBs among SDSS WDMS binaries of $35 \pm 12\%$ obtained here still represents a lower limit. However, as mentioned in the Introduction, the relative number of PCEBs may be a function of the spectral type of the secondary.

5.3. Dependence on the secondary star spectral type

Recently, Politano & Weiler (2006) suggested a test for the disrupted magnetic braking scenario, i.e. the hypothesis that magnetic braking is not active in PCEBs which contain a fully convective companion star. Their calculations predict that the relative number of PCEBs among WDMS binaries should drastically increase for secondary star masses below $M_{\text{sec}} = 0.35 M_{\odot}$. Our results are consistent with that prediction. Among 9 WDMS binaries with spectral type M3 or earlier we find only one strong PCEB candidate while the PCEB identification rate among WDMS binaries containing later secondaries (M4–M6) is 8/17. According to the Poisson statistic, the relative numbers of PCEBs among SDSS WDMS binaries are 0.111 ± 0.111 (for M0–M3) and 0.471 ± 0.166 (for M4–M6). Combining these values we obtain a significance of 1.8σ for the hypothesis of having two different distributions. Interestingly, a potential difference between the secondary star spectral types in close and wide WDMS binaries was also suggested by Farihi et al. (2005), who found, subject to small num-

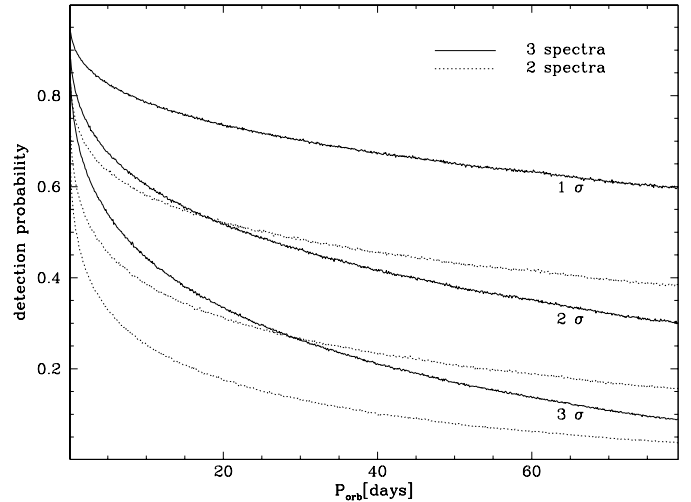


Figure 8. Detection probability versus orbital period for 2 and 3 spectra taken randomly in one semester but not in the same night. We here assumed $M_{\text{wd}} = 0.6 M_{\odot}$ and $M_{\text{sec}} = 0.3 M_{\odot}$. The 1 – 3σ labels refer to the detection level of radial velocity variations. Apparently, using our 3σ criterion to select strong PCEB candidates for further follow-up observations leads to final a sample that is biased toward shorter orbital periods. However, only 3 spectra are needed to identify 15–30% of the PCEBs with longer orbital periods ($P_{\text{orb}} \gtrsim 20$ days) and our strategy can therefore certainly be used to also constrain the orbital period distribution of long orbital period PCEBs.

ber statistics, that the median secondary spectral type of close binaries is one spectral class later than that of the wide binaries. While keeping in mind the well known problems resulting from low number statistics, these results may represent first indications for a discontinuity in the relative number of PCEBs among WDMS binaries as predicted by Politano & Weiler (2006). However, further observations are certainly needed to confirm or disprove the observed tendency.

5.4. Predicted evolution of SDSS J1047+0523 and SDSS J1414–0132

As shown by Schreiber & Gänsicke (2003) knowing the mass and effective temperature of the white dwarf, its orbital period, and at least reasonable estimates for the mass and the radius of the secondary one can determine the age of the PCEB, the orbital period of the future semi-detached system (i.e. a cataclysmic variable) and the time the PCEB evolution takes for a given system.

To that end, we here first follow Schreiber & Gänsicke (2003) by using the white dwarf cooling tracks of Wood (1995) to determine the white dwarf cooling ages of SDSS J1047+0523 and SDSS J1414–0132. Using the white dwarf parameters given in Table 1 and interpolating the cooling tracks we get $t_{\text{cool}} \sim 2.1 \pm 1 \times 10^8$ yrs and $t_{\text{cool}} \sim 3.9 \pm 1.1 \times 10^8$ yrs for SDSS J1047+0523 and SDSS J1414–0132 respectively.

The determination of the mass and the radius of the secondary is much more challenging as the inclination of these two systems is unconstrained. We use the empirical spectral type-radius-mass (Sp-R-M) relation derived

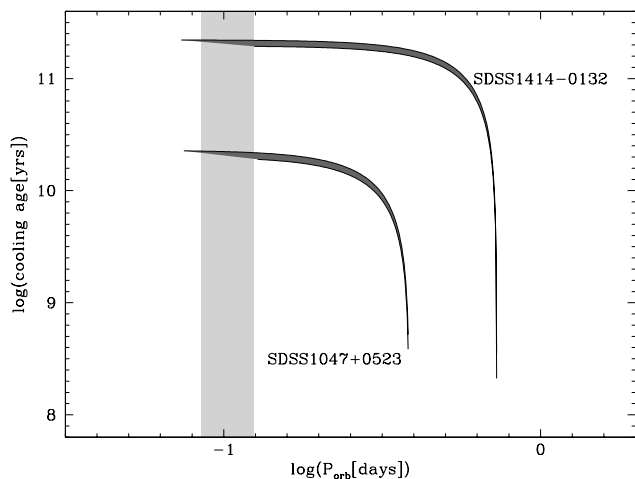


Figure 9. The PCEB evolution of SDSS J1047+0523 and SDSS J1414-0132. Starting at their current orbital periods of $P_{\text{orb}} = 17.48$ h and $P_{\text{orb}} = 9.17$ h the systems evolve towards shorter orbital period due to angular momentum loss by gravitational radiation. The companion stars in SDSS J1047+0523 and SDSS J1414-0132 will fill their Roche-lobes in $1.7 \pm 0.3 \times 10^{10}$ yrs and $1.8 \pm 0.2 \times 10^{11}$ yrs, respectively, and turn these PCEBs into cataclysmic variables. This will happen at very similar orbital periods, 0.090 ± 0.013 days for SDSS J1047+0523 and 0.085 ± 0.015 for SDSS J1414-0132.

in Paper I (Sect. 3.4) to estimate values of the mass and radius of the secondary. Apparently, the scatter around this empirical relation is quite large (Paper I, Fig. 7) and therefore the obtained values should be generally considered as uncertain. However, in the case of SDSS J1414-0132 and SDSS J1047+0523 the distance estimates based on the white dwarf (d_{WD}) and those derived using the empirical Sp-R-M relation agree quite well which suggests that the obtained values are plausible (for a detailed discussion of the spectral type-mass-radius relation see Paper I). As both secondaries are of the spectral type M5 the empirical relation gives $M_{\text{sec}} = 0.216M_{\odot}$ and $R_{\text{sec}} = 0.258R_{\odot}$. For our theoretical analysis we adopt rather broad ranges of possible values to account for the described uncertainties, i.e. $M_{\text{sec}} = 0.20 - 0.23M_{\odot}$ and $R_{\text{sec}} = 0.2 - 0.3R_{\odot}$.

According to the standard scenario of CV evolution, magnetic braking gets disrupted when the secondary stars becomes fully convective (e.g. Verbunt & Zwaan, 1981) and, hence, gravitational radiation is the only angular momentum loss mechanism acting in systems with a low mass ($M_{\text{sec}} \lesssim 0.3M_{\odot}$) secondary star. The evolution of SDSS J1047+0523 and SDSS J1414-0132 according to this scenario and taking into account the uncertainties discussed above, is shown in Fig. 9. Both systems will become CVs in or slightly below the 2–3 h orbital period gap and for both systems the evolution will take longer than a Hubble-time. Therefore, according to Schreiber & Gänsicke (2003), they are not representative for progenitors of the current CV population.

6. Summary

We have obtained ESO-VLT/FORS2 spectroscopy of 26 WDMS binaries found in SDSS. Clear radial velocity variations led to the identification of 9 strong PCEB candidates, which gives a hit-rate of $35 \pm 12\%$. We analysed the PCEB detection probability of our strategy and conclude that (although a bias towards short orbital period systems is inevitable) our survey is sensitive to the predicted long orbital period distribution of PCEBs. While we find 8 PCEB candidates among 17 systems with M4 or later secondary stars only one PCEB candidate could be identified among 9 WDMS binaries containing earlier secondary stars. Although suffering from low number statistics, one may interpret this results as a first indication for a discontinuity in the dependence of the relative number of PCEBs among WDMS binaries on the spectral type of the secondary.

We determined the orbital periods for two of the PCEBs identified here, SDSS J1047+0523 and SDSS J1414-0132, from Magellan-Clay/LDSS3 spectroscopy to be to be 9.17 h and 17.48 h respectively. Both systems will enter the semi-detached CV state in or below the orbital period gap. This evolution will last longer than the Hubble time and both systems are therefore different than the progenitors of the current CV population.

Acknowledgements. MRS acknowledges support from FONDECYT (grant 1061199), DIPUV (project 35), and the Center of Astrophysics in Valparaiso.

References

- Adelman-McCarthy, J. K., Agüeros, M. A., Allam, S. S., et al. 2007, *ApJS*, 172, 634
- Adelman-McCarthy, J. K. & for the SDSS Collaboration. 2007, *ArXiv e-prints*, 707
- Andronov, N., Pinsonneault, M., & Sills, A. 2003, *ApJ*, 582, 358
- Aungwerojwit, A., Gänsicke, B. T., Rodríguez-Gil, P., et al. 2007, *A&A*, 469, 297
- Beer, M. E., Dray, L. M., King, A. R., & Wynn, G. A. 2007, 375, 1000
- Bergeron, P., Wesemael, F., Lamontagne, R., et al. 1995, *ApJ*, 449, 258
- Eisenstein, D. J., Liebert, J., Harris, H. C., et al. 2006, *ApJS*, 167, 40
- Farihi, J., Becklin, E. E., & Zuckerman, B. 2005, *ApJS*, 161, 394
- Fontaine, G., Brassard, P., & Bergeron, P. 2001, *PASP*, 113, 409
- Gänsicke, B. T., Jordan, S., Beuermann, K., et al. 2004, *ApJ Lett.*, 613, L141
- Horne, K. 1986, *PASP*, 98, 609
- Howell, S. B., Nelson, L. A., & Rappaport, S. 2001, *ApJ*, 550, 897
- King, A. R. 1988, *QJRAS*, 29, 1
- Koester, D., Napiwotzki, R., Voss, B., Homeier, D., & Reimers, D. 2005, *A&A*, 439, 317
- López-Morales, M. 2007, *ApJ*, 660, 732
- Marsh, T. R. 1989, *PASP*, 101, 1032
- Marsh, T. R., Robinson, E. L., & Wood, J. H. 1994, *MNRAS*, 266, 137
- Morales-Rueda, L., Marsh, T. R., Maxted, P. F. L., et al. 2005, 359, 648
- Morris, M. 1981, *ApJ*, 249, 572
- Nelemans, G. & Tout, C. A. 2005, *MNRAS*, 356, 753
- Nelemans, G., Verbunt, F., Yungelson, L. R., & Portegies Zwart, S. F. 2000, *A&A*, 360, 1011
- Osterbrock, D. E., Fulbright, J. P., & Bida, T. A. 1997, *PASP*, 109, 614
- Osterbrock, D. E., Fulbright, J. P., Martel, A. R., et al. 1996, *PASP*, 108, 277
- Paczynski, B. 1976, in *IAU Symp. 73: Structure and Evolution of Close Binary Systems*, 75
- Pinsonneault, M. H., Andronov, N., & Sills, A. 2002, in *The Physics of Cataclysmic Variables and Related Objects*, ed. B. T. Gänsicke, K. Beuermann, & K. Reinsch (ASP Conf. Ser. 261), 208–216

Politano, M. & Weiler, K. P. 2006, ApJ Lett., 641, L137
 Rebassa-Mansergas, A., Gaensicke, B. T., Rodriguez-Gil, P., Schreiber, M. R., & Koester, D. 2007, ArXiv e-prints, 707
 Ribas, I. 2006, Ap&SS, 304, 89
 Scargle, J. D. 1982, ApJ, 263, 835
 Schreiber, M. R. & Gänsicke, B. T. 2003, A&A, 406, 304
 Schreiber, M. R., Nebot Gomez-Moran, A., & Schwöpe, A. D. 2007, in Astronomical Society of the Pacific Conference Series, Vol. 372, Astronomical Society of the Pacific Conference Series, ed. A. Napiwotzki & M. R. Burleigh, 459–+
 Shimansky, V., Sakhibullin, N. A., Bikmaev, I., et al. 2006, A&A, 456, 1069
 Silvestri, N. M., Lemagie, M. P., Hawley, S. L., et al. 2007, ArXiv e-prints, 704
 Southworth, J., Gänsicke, B. T., Marsh, T. R., et al. 2006, MNRAS, 373, 687
 Southworth, J., Marsh, T. R., Gänsicke, B. T., et al. 2007, MNRAS, 382, 1145
 Taam, R. E. & Bodenheimer, P. 1989, ApJ, 337, 849
 Taam, R. E. & Ricker, P. M. 2006, ArXiv Astrophysics e-prints
 Taam, R. E. & Sandquist, E. L. 2000, ARA&A, 38, 113
 Tappert, C., Gänsicke, B. T., Schmidtobreick, L., et al. 2007, A&A, 474, 205
 van den Besselaar, E. J. M., Greimel, R., Morales-Rueda, L., et al. 2007, 466, 1031
 van den Besselaar, E. J. M., Roelofs, G. H. A., Nelemans, G. A., Augusteijn, T., & Groot, P. J. 2005, 434, L13
 Verbunt, F. & Zwaan, C. 1981, A&A, 100, L7
 Webbink, R. F. 1984, ApJ, 277, 355
 Webbink, R. F. 2007, ArXiv e-prints, 704
 Willems, B. & Kolb, U. 2004, A&A, 419, 1057
 Wood, M. A. 1995, in White Dwarfs, ed. D. Koester & K. Werner, LNP No. 443 (Heidelberg: Springer), 41–45

Table 3. Radial velocities measured from the Na I $\lambda\lambda$ 8183.27, 8194.81 doublet in the ESO/VLT and SDSS spectra. The radial velocities obtained from SDSS data is indicated by the HJD set in italics.

HJD	RV [km s ⁻¹]	HJD	RV [km s ⁻¹]
SDSS J0017–0024		SDSS J1126+0108	
2453978.64799	-26.7±5.0	2454142.80234	-7.7±4.9
2453982.67389	-18.3±5.5	2454155.62142	-12.1±4.7
<i>2452518.922000</i>	-1.8±16.7	<i>2451614.80814</i>	-1.1±15.4
<i>2452559.785000</i>	-36.3±15.5	SDSS J1222+0934	
SDSS J0228–0740		2454142.831916	-50.4±4.6
2453983.68162	4.0±8.0	2454156.875771	-48.3±4.5
2453983.69278	9.9±7.5	SDSS J1252–0206	
-	-16.9±21.0	2454142.84647	-30.4±6.4
SDSS J0320–0638		2454169.68656	-26.7±5.6
2454030.85227	240.0±5.9	2454185.58421	-31.1±6.0
2454086.60870	204.1±7.0	<i>2451694.70928</i>	-33.3±24.0
2454124.60190	212.1±6.0	SDSS J1414–0132	
<i>2451924.67646</i>	172.9±24.8	2454142.86192	154.2±7.3
SDSS J0819+0604		2454169.71281	-65.9±5.7
2454030.87927	26.4±5.7	2454180.89912	137.7±7.8
2454055.83644	39.2±6.0	-	35.2±24.9
<i>2452963.00286</i>	19.8±17.1	SDSS J1425+0230	
SDSS J0833+0702		2453982.48632	102.6±8.4
2454055.85156	83.5±5.5	2453983.49473	95.3±19.7
2454059.82430	121.6±5.9	<i>2451999.89365</i>	101.1±26.3
<i>2452963.98436</i>	194.5±18.3	SDSS J1506–0120	
SDSS J0855+0447		2453965.51719	41.8±5.3
2454059.83910	73.3±7.3	2453982.50834	-85.4±5.6
2454060.84131	-11.7±7.0	<i>2452426.79507</i>	61.2±18.6
<i>2452670.87671</i>	15.8±21.1	SDSS J2045–0509	
SDSS J0924–0017		2453978.52649	-48.4±5.8
2454067.842758	15.4±4.5	2453978.53830	-42.5±5.9
2454086.796712	14.7±5.2	2453981.61523	-21.6±5.2
SDSS J0939+0511		<i>2452145.71287</i>	12.1±21.2
2454086.81276	103.7±6.8	SDSS J2050–0002	
2454087.84233	86.5±5.4	2453998.625440	34.1±9.1
<i>2452710.81094</i>	130.1±24.9	2454001.522929	15.0±5.8
SDSS J0951+0255		<i>2452466.81829</i>	30.8±37.5
2454086.82795	13.6±7.4	SDSS J2123+0024	
2454099.81594	20.1±5.6	2453978.55706	56.1±14.5
<i>2451908.91909</i>	37.0±18.3	2453981.63252	-91.6±7.8
SDSS J1009–0028		<i>2452523.69331</i>	198.2±35.6
2454086.84235	-2.6±9.0	SDSS J2156–0002	
2454112.83168	-2.6±8.8	2453992.53760	-18.0±5.4
<i>2451909.91534</i>	-48.0±23.7	2453998.64315	-98.9±6.4
SDSS J1043+0603		2454004.55526	21.6±5.1
2454117.75282	46.2±7.0	<i>2452075.89855</i>	-68.1±15.9
2454149.70110	48.0±7.2	SDSS J2203–0017	
<i>2452644.01881</i>	37.7±22.9	2453978.57300	-48.7±6.4
SDSS J1047+0523		2453982.53714	-61.9±7.2
2454142.77188	-19.4±8.9	<i>2452173.63031</i>	-20.9±29.5
<i>2452339.82994</i>	218.0±19.8	SDSS J2312+0101	
SDSS J1101+1222		2453978.59006	14.7±4.7
2454142.78686	-16.1±9.9	<i>2451811.73493</i>	18.3±16.2
2454155.63799	-22.0±8.8	SDSS J2324–0931	
2454167.69909	-23.1±6.9	2453963.82187	7.3±5.5
2454169.67087	-25.3±6.0	<i>2452203.63065</i>	-1.8±18.7
2454184.61366	-40.3±6.3		
<i>2453119.74299</i>	-56.8±19.8		

Table 4. Radial velocities measured from the Na I $\lambda\lambda$ 8183.27, 8194.81 doublet in the Clay/LDSS3 spectra of the two PCEB candidates SDSS J1047+0523 and SDSS J1414-0132.

HJD	RV [km s ⁻¹]	HJD	RV [km s ⁻¹]
SDSS J1047+0523		SDSS J1414-0132	
2454237.54059	214.7±10.4	2454237.616516	190.1±11.0
2454237.64147	0.0±20.8	2454237.625451	192.7±12.1
2454238.48000	-127.5±9.5	2454238.587532	-78.8±11.2
2454238.51267	-107.0±17.2	2454238.736750	-100.0±10.5
2454238.55507	-72.5±17.1	2454239.576845	4.8±14.9
2454238.66262	240.7±9.8	2454239.686966	160.5±7.0
2454239.54693	6.6±19.8	2454239.752785	209.9±17.2
2454239.58773	-119.4±11.9	2454240.498312	189.0±11.8
2454239.61468	-129.7±8.8	2454240.569119	180.2±8.8
2454239.64270	-133.0±10.0	2454240.579801	181.0±11.0
2454240.46501	-31.9±11.6	2454240.671845	37.0±7.7
2454240.51077	109.5±10.5	2454240.696022	8.1±10.4
2454240.59002	218.7±10.5	2454240.753426	-64.1±11.4
2454240.64421	162.7±11.7	2454240.762373	-62.6±12.0
2454240.65411	163.4±9.6	2454240.790358	-108.4±7.9
		2454240.801040	-119.1±13.8